Synthesis, Photoluminescence, and Adsorption of CdS/Dendrimer Nanocomposites

X. C. Wu, A. M. Bittner,* and K. Kern

Max-Planck-Institut für Festkörperforschung, Heisenbergstrasse 1, D-70569 Stuttgart, Germany

Received: August 31, 2004; In Final Form: October 20, 2004

CdS/dendrimer nanocomposites can be synthesized from methanolic Cd^{2+} and S^{2-} with amine-terminated polyamidoamine dendrimers of generation 8 (G8NH₂) as stabilizers. By controlling the preparation conditions, nanoparticles with diameters $\leq$ 2 nm can be obtained with a narrow size distribution. They show blue photoluminescence at ~450 nm. We studied the effects of various additives on the photoluminescence and elucidated its mechanism. Stable aggregates of two to three G8NH₂ molecules with several CdS nanoparticles form; the particles are located at the surface of the G8NH₂ molecules. The adsorption of the CdS/G8NH₂ nanocomposites on flat substrate surfaces is determined by the substrate chemistry. The hydrophilic nature of G8NH₂ results in weak affinity to graphite but strong affinity to hydroxy-terminated substrates such as mica, oxidized silicon wafers, and carboxylate-terminated monolayers. Patterning of nanocomposites on these hydrophilic substrates is achieved by the microcontact printing method. We propose to use only one molecule, a large dendrimer, to control the nanoparticle formation and also the immobilization of the synthesized nanoparticle/dendrimer composites.

1. Introduction

Semiconductor nanoparticles show unique size-dependent optical properties and are of great interest for applications in optoelectronics, photovoltaics, and biological sensing.[1,2] Various chemical synthetic methods have been developed to prepare such nanoparticles. Wet chemical syntheses can be realized with so-called "stabilizers", which cap the surface of the nanoparticles during their growth, or by confinement in nanoreactors. Two different approaches have been developed to synthesize high-quality semiconductor nanoparticles with stabilizers. One is an organometallic synthesis based on the high-temperature thermolysis of precursors, first reported by Murray et al. in 1993,[3] and further improved later on.[4-6] An alternative synthesis employs polyphosphates[7] or thiols[8] in aqueous media. For the case of nanoreactors, various cage-shaped functional materials such as reverse micelles,[9] diblock copolymers,[10] and vesicles,[11] etc., are used to control the growth of nanoparticles. However, their quality, especially concerning the band edge exciton emission, has not yet reached that of nanoparticles generated by the other approaches.

Apart from having good quality, nanoparticles should easily form films or assemble on substrates for potential applications in optics and in optoelectronics. Here, the chemical properties of the nanoparticle surface play a very important role. Often, the organic stabilizers that are used to control the growth of nanoparticles are not suitable for forming films or for the adsorption of the nanoparticles to a substrate: An additional molecular compound is needed to displace the original stabilizers and to bind the particles to the substrate,[12,13] or a chemically reactive substrate must be present.[14] Could one material fulfill these two functions? Polyamidoamine (PAMAM) dendrimers, first synthesized by Tomalia in 1985, are highly branched molecules with well-defined molecular weight and size.[15] Hence, they are monodisperse molecular-level templates for chemical syntheses.[16-19] They are composed of core, repetitive units and terminal groups, each with a different chemical functionality. A dendrimer can selectively bind a well-defined number of noble metal ions, and it is a good nanoreactor for the reductive synthesis of the corresponding metal clusters.[16-18] Recently, syntheses of metal, semiconductor, and oxide nanoparticles stabilized by dendrimers were reported,[19-27] in three cases CdS nanoparticles.[19,23,27] According to the relative location of nanoparticles at or in dendrimers, three different types of nanocomposites exist,[28] i.e., nanoparticles inside dendrimers ("internal type"), outside ("external type"), or both ("mixed type"). Which type is formed is controlled by the size and shape of the dendrimers, by the interactions between the metal ions and the dendrimers, and by the reaction pathways for the formation of the nanocomposites. Therefore, dendrimers can be used either as nanoreactors (templates with internal cavities, hence, the internal type) or as stabilizer-like templates (external type).

In addition, dendrimers can form layers on substrates. These layers attach by electrostatic forces, hydrogen bonds, van der Waals forces, metal–ligand interactions, or covalent bonds between the terminal groups and a substrate.[29-32] Apart from such 2D assemblies, the 3D deposition of dendrimer-based systems with a layer-by-layer deposition technique has been reported.[29,33] Moreover, dendrimers can be arranged in patterns via microcontact printing.[34-36] Therefore, dendrimers can do both, i.e., on one hand act as stabilizer-like templates for the formation of the nanoparticles and on the other hand immobilize the particles on a substrate. In our study we used CdS nanoparticles, which have been prepared in various media and studied widely,[37-42] as model guests and studied their synthesis at dendrimer hosts, their optical properties, the morphologies of the CdS/dendrimer nanocomposites, and their adsorption and patterning.

In the following section, we present our synthetic approach to CdS/dendrimer composites. Section 3 features the pronounced influence of metal cations, sulfide, and several organic molecules on the CdS photoluminescence. When our synthesized composite dispersion is kept at 25 °C, aging (particle growth) is observed. This process and its influence on the luminescence are discussed in section 4. Atomic force microscopy (AFM)

CdS/Dendrimer Nanocomposites

J. Phys. Chem. B, Vol. 109, No. 1, 2005 **231**

results on morphology, adsorption, and patterning of the composites are given in section 5. Section 6 concludes by providing a summary and an outlook.

2. Experimental Section

We employed "G8NH$_2$", an amine-terminated, generation 8 polyamidoamine starburst dendrimer (8% (w/w) in methanol, Dendritech). Cd(CH$_3$COO)$_2$, Pb(CH$_3$COO)$_2$, Zn(CH$_3$COO)$_2$, hexadecylamine (CH$_3$(CH$_2$)$_{15}$NH$_2$), Na$_2$S (all of analytical grade), and mercaptohexadecanoic acid (HOOC(CH$_2$)$_{15}$SH) (90%) were from Aldrich. Dodecanethiol (CH$_3$(CH$_2$)$_{11}$SH; >98%), methanol (analytical grade), NaOH (analytical grade), 25% NH$_4$OH in water (VLSI Selectipur), 31% H$_2$O$_2$ in water (VLSI Selectipur), and 30% HCl (Suprapur) were from Merck. Water (18.2 MΩ cm) was from a Millipore system.

Cd^{2+}, S^{2-}, and G8NH$_2$ were mixed at room temperature under an argon atmosphere to obtain CdS/G8NH$_2$ nanocomposites. A typical preparation of CdS/G8NH$_2$ nanocomposites with an initial Cd^{2+}/S^{2-} molar ratio of 1:1 was as follows: a 50 μL G8NH$_2$ solution was diluted with methanol to 2.5 mL (5.5 μM G8NH$_2$); then 2.5 mL of 2 mM Cd(CH$_3$COO)$_2$ and 2.5 mL of 2 mM Na$_2$S in methanol were added sequentially. The initial ratio Cd^{2+}/G8NH$_2$ was 360; this ratio was used for all syntheses. For adsorption, printing, and transmission electron microscopy experiments, the solution was dialyzed against pure methanol for 1 day.

Silicon wafers (orientation (100), from Crystal, Berlin, Germany) were terminated by silicon oxide and OH groups by the standard RCA procedure: 15 min immersion into a 1:1:5 mixture of 25% NH$_4$OH, 31% H$_2$O$_2$, and water at 65–75 °C; rinsing with water; 15 min immersion into a 1:1:5 mixture of 30% HCl, 31% H$_2$O$_2$, and water at 65–75 °C; rinsing with water. Highly oriented pyrolytic graphite (HOPG) of ZYA quality was from NTMDT, Moscow. Gold/mica substrates were obtained by depositing 150–200 nm of gold (0.2 nm s^{-1}) on freshly cleaved 300 °C hot mica at a base pressure of 10^{-5} mbar. Before use, gold substrates were flame-annealed at dark red glow with a small butane flame. HOOC(CH$_2$)$_{15}$S/gold was prepared by overnight immersion of annealed gold/mica in 1 mM mercaptohexadecanoic acid in ethanol.

UV/visible absorption spectra were obtained with a Perkin-Elmer Lambda 2 spectrometer; photoluminescence and excitation spectra with a Perkin-Elmer LS 50B spectrometer. Photoluminescence quantum yields were determined by comparison with a Coumarin 47 solution. Transmission electron micrographs of composite-covered grids were recorded at 200 kV with a Philips CM 200. For the time-resolved measurements, the pulsed output of a frequency-doubled titanium–sapphire laser (370 nm, 150 fs, 76 MHz) was used for sample excitation. The photoluminescence signal was spectrally dispersed by a monochromator and temporally resolved by a synchroscan streak camera system (Hamamatsu). The time resolution of the system was 10 ps. Atomic force microscopy images were obtained in intermittent contact (IC) mode with a Thermomicroscopes Autoprobe M5. Probes were ultrasharp noncontact silicon cantilevers from MikroMasch or from Nanosensors. Microcontact printing was carried out as detailed in ref 75.

3. CdS/Dendrimer Photoluminescence and the Influence of Additives

PAMAM dendrimers contain three types of amine groups, NH$_2$, NR$_3$, and CONHR (where R is a linear hydrocarbon chain). All of them can be binding sites for Cd^{2+} ions. Their binding affinity to Cd^{2+} ions is expected to follow the order
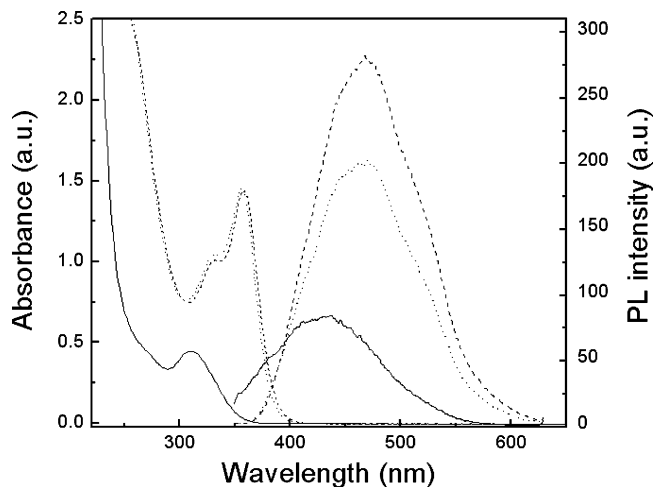

Figure 1. Absorption and photoluminescence (PL; excitation at 320 nm) spectra of of CdS/G8NH$_2$ nanocomposites in methanol with Cd^{2+}/S^{2-} ratios of 3:1 (solid), 1:1 (dashed), and 1:2 (dotted). Recorded 1 h after synthesis.
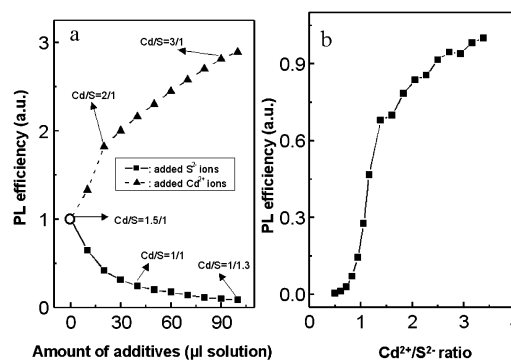

Figure 2. Effects of added Cd^{2+} or S^{2-} ions (a) and of Cd^{2+}/S^{2-} ratios (b) on the integrated PL efficiency. The open circle in a marks the initial condition, a Cd^{2+}/S^{2-} ratio of 1.5.

NH$_2$ > NR$_3$ > CONHR.[43,44] Unlike Cu^{2+} and Pd^{2+}, etc., the binding of Cd^{2+} ions to amine groups does not result in any new features in UV/visible absorption spectra. This excludes the possibility of controlling the load factor of Cd^{2+} in dendrimers by a simple spectroscopic titration. Hence, we evaluated the loading of Cd^{2+} by monitoring the formation of CdS nanoparticles. Assuming two NH$_2$ groups per Cd^{2+} ion, we mixed Cd^{2+}, S^{2-} (ratio 1:1), and G8NH$_2$ in the following ratios: (A) Cd^{2+} binding only NH$_2$ groups (512 Cd^{2+}/G8NH$_2$); (B) Cd^{2+} binding NH$_2$ and the outermost shell of NR$_3$ groups (768 Cd^{2+}/G8NH$_2$); (C) Cd^{2+} binding NH$_2$ and all NR$_3$ (1023 Cd^{2+}/G8NH$_2$); (D) Cd^{2+} binding NH$_2$, all NR$_3$, and a part of the CONHR groups (1535 Cd^{2+}/G8NH$_2$). Only the first case, A, resulted in a stable dispersion (no precipitation). This suggests that Cd^{2+} ions mainly interact with the terminal NH$_2$ groups; hence, the dendrimer does not act as cavity template (nanoreactor). For all following experiments, we fixed the Cd^{2+}/G8NH$_2$ ratio to 360. We varied the Cd^{2+}/S^{2-} ratios systematically and also added other ions and molecules in various relative quantities. The results of these experiments are reported in the following subsections. For comparison, a standard result for absorption and photoluminescence of our CdS/G8NH$_2$ composites is shown in Figure 1.

Effect of Additives on the Blue Photoluminescence. We found that the photoluminescence (PL) was sensitive to the Cd^{2+}/S^{2-} ratios. Figure 2a shows the variations in the PL yield for a sample with an initial Cd^{2+}/S^{2-} ratio of 1.5:1 after adding Cd^{2+} and S^{2-}, respectively. The final Cd^{2+}/S^{2-} ratios after the
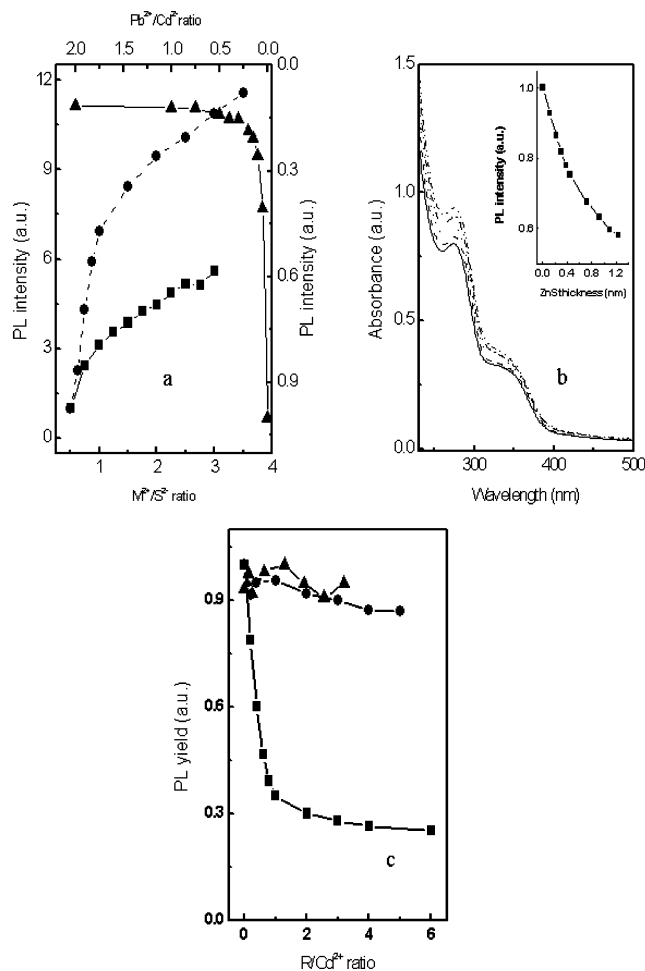
Figure 3. (a) Effects of adding Cd^{2+} (filled circles), Zn^{2+} (squares), and Pb^{2+} (triangles, intensity scale at right) on the PL efficiency of $CdS/G8NH_2$ (initial Cd^{2+}/S^{2-} ratio = 1:2). (b) Evolution of absorption spectra for $CdS-ZnS$ core–shell structures with calculated shell thicknesses of 0, 0.17, 0.34, 0.59, and 1 nm. Inset: Dependence of the PL efficiency on the thickness of the ZnS shell. (Cd^{2+}/S^{2-} ratio = 1:1). (c) Dependence of the PL efficiency on the ratio R (functional groups)/ Cd^{2+}: 2 mM $CH_3(CH_2)_{11}SH$ (squares), 2 mM $CH_3(CH_2)_{15}NH_2$ (circles), and 10 μM $G4NH_2$ (triangles). Cd^{2+}/S^{2-} ratio = 1:1; solvent methanol.

addition are marked for some values. While adding Cd^{2+} increased the PL efficiency, adding S^{2-} decreased it. Samples with an excess of S^{2-} ions (Cd^{2+}/S^{2-} ratio less than 1:2) were unstable—with respect to precipitation—compared to those with an excess of Cd^{2+} ions. To obtain the dependence of the PL yield on the Cd^{2+}/S^{2-} ratios, we added Cd^{2+} ions to a sample with an initial Cd^{2+}/S^{2-} ratio of 1:2 (see Figure 2b). The PL intensity increased very strongly for Cd^{2+}/S^{2-} ratios from 1 to 1.5. It tended to saturate at higher ratios. Hence, the most efficient blue PL was found for $Cd^{2+}/S^{2-} > 1.5$.

Adding Zn^{2+} ions, similar to the case of adding Cd^{2+} ions, led to an increase of the PL, while adding Pb^{2+} quenched it (see Figure 3a). Furthermore, by sequential addition of Zn^{2+} and S^{2-} ions to a CdS nanoparticle solution, core–shell-type structures formed as verified by gradual small red shifts of absorption spectra (Figure 3b).[45-47] Apart from the formation of core–shell structures, isolated ZnS nanoparticles at the surface of CdS nanoparticles and $Zn_xCd_{1-x}S$ ($0 < x < 1$) alloys may form, too, when preparing such binary compounds. Controlling experimental parameters can avoid unwanted structures. Pure ZnS nanoparticles stabilized by $G8NH_2$ show an obvious exciton peak at ~250 nm. The absence of this exciton peak excludes the formation of isolated ZnS nanoparticles. The
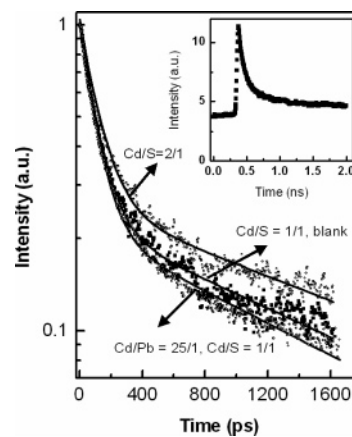

Figure 4. PL decay curves detected at the peak position (450 nm) of the blue PL for a blank $CdS/G8NH_2$ sample, for added Pb^{2+}, and for added Cd^{2+}. The dots are experimental points, while the solid lines show biexponential theoretical fits. Inset: Example for entire decay curve; the excitation pulse arrived at ~0.35 ns.

red shift of band gaps rules out the existence of $Zn_xCd_{1-x}S$ alloys since the band gap would then blue-shift with increasing Zn^{2+} content for such alloys.[37,41] We observed that increasing thickness of the ZnS shell in the CdS–ZnS core–shell structures lead to decreasing PL intensity (Figure 3b inset).

These results can be a first hint for the PL mechanism. To obtain more information, we tried to passivate electron trap states with electron-donating additives. This should be possible because the PL shows a large Stokes shift from the absorption band gap, pointing to PL from defect-state emission. The donor $CH_3(CH_2)_{11}SH$ binds strongly to CdS nanoparticles and has been used to replace weakly interacting stabilizers on the surface of CdS nanoparticles.[9] Long-chain amines have been used as donors to interact with surface Cd^{2+} ions (acceptors) of CdS nanoparticles in order to further optimize the band gap PL.[4] Figure 3c reports the dependence of the PL intensity on the ratio of R(functional group)/Cd^{2+}. Linear $CH_3(CH_2)_{15}NH_2$ and amine-terminated dendrimers had no obvious effects, while $CH_3(CH_2)_{11}SH$ quenched the PL efficiently (for ratios from 0 to ~1, the PL intensity decreased drastically, while further addition had no obvious influence).

Effect of Additives on the Photoluminescence Decay. The PL efficiency is determined by both radiative and nonradiative processes. For nanoparticles, due to an increased surface area where various defects dominate, nonradiative processes play an important role in the excitation decay. Opening up new nonradiative pathways decreases the PL efficiency, while elimination of nonradiative pathways increases the efficiency. At the same time, also the kinetics of the PL can be influenced. We changed the PL decay time by adding Pb^{2+} and Cd^{2+} (see Figure 4). The rise time of the PL (Figure 4 inset) was very fast (within the time resolution of the measurement system), indicating very short trapping times for photoinduced electrons and holes. The complete decay process took longer than our 2 ns time window; some residual PL still existed when the next laser pulse arrived. PL decay curves $I_{em}(t)$ were fitted with a biexponential function, $I_{em} = A_1 \exp(-t/\tau_1) + A_2 \exp(-t/\tau_2)$ in a 2 ns time window, yielding the fitting parameters in Table 1. Multiexponential decay has been often observed both for band edge exciton PL[45,48-51] and for trapped-state PL at room temperature.[48-50,52,53] This has been ascribed, due to distributions of both size and shape of nanocrystals, to emitting states with different lifetimes and to detrapping and repopulation of carriers at different energies.[48-53] We believe that our case (for a 2 ns

CdS/Dendrimer Nanocomposites

J. Phys. Chem. B, Vol. 109, No. 1, 2005 **233**

TABLE 1: Fitting Parameters of the Biexponential PL Decay Curves (See Figure 4; Intensity $= A_1 \exp(-t/\tau_1) + A_2 \exp(-t/\tau_2)$)

samples	A_1	τ_1 (ps)	A_2	τ_2 (ps)
blank (Cd^{2+}/S^{2-} = 1:1)	0.78	102 ± 1	0.22	1843 ± 50
added Cd^{2+} (Cd^{2+}/S^{2-} = 2:1)	0.78	114 ± 2	0.26	2179 ± 63
added Pb^{2+} (Cd^{2+}/S^{2-} =1:1, Pb^{2+}/Cd^{2+} = 1:25)	0.81	96 ± 1	0.29	1662 ± 35

time window) comprises mainly two emitting states with close emission energies. The fast decay part ($\sim$0.1 ns) corresponds to an emitting state with a short lifetime, while the slow one ($\sim$1.8 ns) stems from an emitting state with a long lifetime. Since the lifetime is determined by both radiative and nonradiative decay, one possibility is that the two states have very different radiative decay times. However, we favor an explanation based on similar radiative, but different nonradiative decay times. This would mean similar defect states in the CdS, but different surface conditions on the nanoparticle, i.e., CdS that is passivated by more or less contact with the dendrimers; more contact means better passivation and slower decay.

Compared with a standard sample ("blank" in Table 1), the PL decay in the presence of added Cd^{2+} slowed slightly, while it accelerated slightly with Pb^{2+}. This helps us to analyze nonradiative processes. Since the solubility constant of PbS (8×10^{-28} mol^2 L^{-2}) is smaller than that of CdS (8×10^{-27} mol^2 L^{-2}), adding Pb^{2+} ions leads to a replacement of Cd^{2+} ions by Pb^{2+} ions and to the formation of PbS. According to our calculation for a 2.2 nm diameter CdS nanoparticle (see Appendix), the formation of a complete PbS monolayer on the surface requires Pb^{2+}/Cd^{2+} > 0.92. In Figure 3a this corresponds to the last two points, where quenching reaches the steady state. For Pb^{2+}/Cd^{2+} < 0.92, we infer the presence of isolated PbS nanoparticles on the surface of the CdS particles. The conduction band offset between bulk CdS and PbS is 1.2 eV.[54] The kinetic energies for electrons and holes in a 2.2 nm diameter CdS particle are 0.72 and 0.24 eV, respectively. Therefore electrons and holes will be trapped in the PbS part (due to larger potential energies for both). The acceleration of the PL decay by adding Pb^{2+} ions indicates that carriers trapped at PL centers of the CdS part further relax to the PbS part of the nanoparticle. This kind of quenching was also observed for HgS nanoparticles adsorbed on the surface of CdS nanoparticles.[38] For the case of added Cd^{2+}, the slight slowing of the decay process indicates that some nonradiative pathways might have been eliminated. Since Cd^{2+} interacts with hole traps in the CdS particle, we infer that sulfur dangling bonds, which form shallow hole traps above the valence band, play an important role in the nonradiative recombination. Adding Cd^{2+} ions should passivate some dangling bonds and thereby increase the PL intensity. In contrast, adding both S^{2-} ions and $CH_3(CH_2)_{11}SH$ molecules shortened the decay process slightly, probably indicating an increase in nonradiative centers.

We suggest the following model: The PL centers are the deep hole traps, and they compete with shallow hole traps for either free or shallow-trapped electrons. If the density of the shallow hole traps is high, their recombination with electrons is preferred, and the PL intensity decreases. Adding S^{2-} ions, on the one hand, covers the surface of the nanoparticle with excess S^{2-} and therefore creates more sulfur dangling bonds; on the other hand, S^{2-} also competes with the NH_2 groups of G8NH$_2$ that bind surface Cd^{2+} (for the stabilization of the nanoparticle) and thus produces a surface with less protective groups. While the latter effect might be responsible for the relatively low stability of nanocomposites with a small Cd^{2+}/

S^{2-} ratio, both effects should yield a nanoparticle surface with more nonradiative centers. The slight shortening of the PL decay times indicates that most photoinduced carriers are directly trapped by nonradiative centers close to the band edge, and therefore do not influence the decay of the defect-state PL. However, some carriers already trapped at PL centers further relax via nonradiative pathways and contribute to the slight shortening of the PL decay.

$CH_3(CH_2)_{11}SH$ molecules show an influence that is similar to that of S^{2-}. Vossmeyer et al. reported that the band edge exciton PL from CdSe nanocrystals decreases when dithiols are bound to the nanocrytstal surface, likely due to perturbation of the electronic structure of the CdSe core.[12] We believe that in our case the $CH_3(CH_2)_{11}SH$ molecules have a similar effect. Note that the molecules are unable to penetrate the CdS, further verifying that the quenching process is mainly surface-related. G4NH$_2$ and $CH_3(CH_2)_{15}NH_2$ are electron donors and mainly influence shallow electron traps. Different from $CH_3(CH_2)_{11}$-SH and S^{2-} ions, they do not increase the density of nonradiative centers and therefore have no obvious influence on the PL.

Adding Cd^{2+} ions, on the one hand, can effectively eliminate shallow hole traps (e.g. sulfur dangling bonds) that compete with deep hole traps (PL centers); on the other hand, surface Cd^{2+} ions can attract NH_2 groups of neighboring G8NH$_2$ molecules to achieve a better passivation of the nanoparticle. This corresponds to the obvious growth of the nanoparticles at higher Cd^{2+}/S^{2-} ratios. Figure 2b suggests that the PL is not much influenced by surplus Cd^{2+} at high Cd^{2+}/S^{2-} ratios; in fact, some of the surplus Cd^{2+} ions can bind to amine groups, which are still available after CdS nanoparticles have formed. Since the solubility product of ZnS (1.6×10^{-23} mol^2 L^{-2}) is larger than that of CdS (8×10^{-27} mol^2 L^{-2}), adding only Zn^{2+} ions will not lead to the formation of a ZnS shell. However, similar to Cd^{2+} ions, Zn^{2+} ions can decrease the number of nonradiative centers to a certain degree and thus increase the PL intensity, though less effectively than Cd^{2+} (due to their different ionic radius). To obtain or to improve band edge exciton emission, core$-$shell nanoclusters with larger band gap material as shell are synthesized to decrease defect-state emission and nonradiative recombination.[45$-$47] Here this concept was also applied. But we did not observe the appearance of band edge exciton emission in our CdS$-$ZnS core$-$shell structures, although the defect-state PL intensity decreased by $\sim$30% for three layers of the ZnS shell. The reason might be incomplete passivation of interface defects due to the large mismatch between the CdS and ZnS lattice constants (7%) and due to unoptimized growth conditions for the ZnS shell.

4. Aging of the CdS/Dendrimer Nanocomposites

The red shift of the absorption spectra of the synthesized CdS/G8NH$_2$ nanocomposites (see Figure 5) shows that further growth occurs during storage at 25 °C ("RT aging"). We found that this growth behavior is sensitive to the Cd^{2+}/S^{2-} ratio in the synthesis. CdS nanoparticles with an initial Cd^{2+}/S^{2-} ratio of 1:1 showed no red shift of the band gaps, but a narrowing of the absorption structures upon RT aging. We interpret this as size-focusing growth: Narrowing of the size distribution occurs when all nanocrystals in a solution are slightly larger than a certain critical size.[55$-$58] Under these conditions, the smaller nanocrystals in the distribution grow faster than the larger ones. CdS nanoparticles with initial Cd^{2+}/S^{2-} ratios of 3:1 and 1:2 showed a narrowing of the absorption structures with a rapid red shift of band gaps at short aging times, but a gradual red shift at longer times. The later stage reflects a size-defocusing
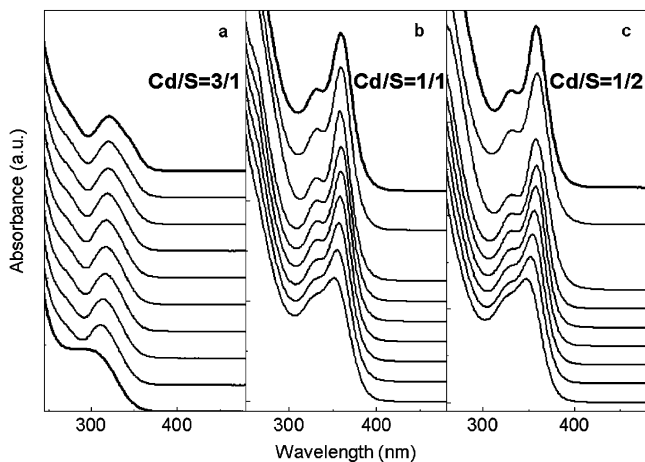
Figure 5. Evolution of absorption spectra of CdS/G8NH$_2$ nanocomposites in methanol after storage at 25 °C (RT aging); spectra at the bottom without aging. (a) Cd/S ratio 3:1; aging, 0 min, 1 h 10 min, 2 h 10 min, 3 h 55 min, 5 h, 6 h, 17 h, 1 day, 3 days, and 6 days. (b, c) ratios of 1:1 and 1:2; aging, 0 min, 10 min, 30 min, 1 h 10 min, 3 h 15 min, 5 h 39 min, 2 days, 6 days, and 7 days.
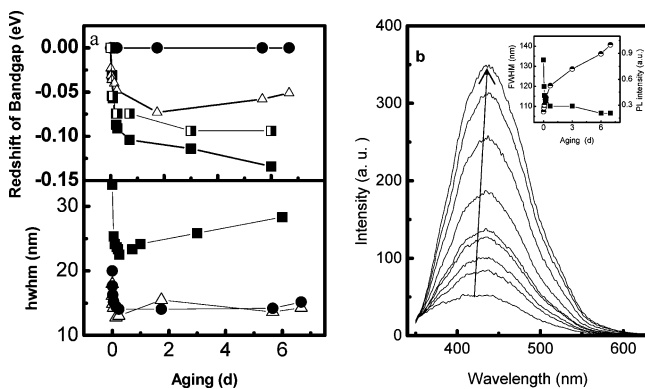

Figure 6. (a) Upper part: Red shift of band gap (solid squares) and PL (half-squares) for a Cd^{2+}/S^{2-} ratio of 3:1 and red shifts of band gaps for Cd^{2+}/S^{2-} ratios of 1:1 (solid circles) and 1:2 (empty triangles), as a function of RT aging. The open circle marks the start of the experiments. Lower part: Variations in half-width at half-maximum of the exciton absorption peak upon aging for Cd^{2+}/S^{2-} ratios of 3:1 (solid squares), 1:1 (solid circles), and 1:2 (empty triangles). (b) Corresponding evolutions of PL spectra (λ_{ex} = 320 nm) for the sample with the Cd^{2+}/S^{2-} ratio of 3:1. Inset: Changes in full width at half-maximum of the exciton absorption peak (solid squares) and in PL intensity (half-filled circles) upon aging.

growth:[55−58] When the monomer concentration (here solvated Cd^{2+} or S^{2-} ions, not nanoparticles) is depleted due to the growth, the critical size (the particle radius in equilibrium with the bulk solution) of the particles becomes larger than the average size, and the distribution broadens because some smaller nanocrystals are shrinking and eventually disappear, while larger ones are still growing (Ostwald ripening). Deviations from the stoichiometric ratio enhance the defocusing growth. Figure 6a shows the red shifts of the band gaps with time. Each band gap E_g was extrapolated from $\sigma h\nu' = (h\nu' - E_g)^{1/2}$ (σ is the extinction coefficient; $h\nu'$ is the energy of the radiation).[59] During 6 days of aging, CdS nanoparticles with an initial Cd^{2+}/S^{2-} ratio of 1:1 showed no increase in average particle size, while those with initial Cd^{2+}/S^{2-} ratios of 3:1 and 1:2 showed an obvious increase in average particle size, indicated by the red shift of E_g.

For samples with a Cd^{2+}/S^{2-} ratio of 3:1, the particle size range coincides with that (diameter < 2 nm) of CdS nanoparticles stabilized with 1-thioglycerol.[60] For the latter, however,

the lowest absorption bands did not shift gradually during the particle growth, but one absorption band was formed at the expense of another (280, 308, and 333 nm). In our case, except for the initial growth stage (the first 70 min), this band shifted from 293 (actually a plateau) to 312 nm, and it showed a gradual red shift from 312 to 321 nm in the subsequent growth. We attribute this difference in growth behavior to different reaction temperatures and stabilizers. For samples with a Cd^{2+}/S^{2-} ratio of 1:1, the lowest absorption band (358 nm) coincides with that of Cd$_{32}$S$_{14}$(SC$_6$H$_5$)$_{36}$·(DMF)$_4$ (DMF = dimethylformamide), a cluster with a 1.5 nm CdS core.[61] We find an obvious peak around 332 nm that is assigned to the second exciton transition of CdS nanoparticles; this peak is not observed for Cd$_{32}$S$_{14}$-(SC$_6$H$_5$)$_{36}$·(DMF)$_4$, which shows a strong broad luminescence at 500 nm that is attributed to an intrinsic excited state of the cluster, since the cluster has an extremely sharp size distribution and a well-defined surface.[61] Although our nanoparticles also show a strong broad emission (centered at 460 nm), the 460 nm emission is here from surface defect states; very narrow band-gap exciton emission for CdS nanoparticles of similar size has been reported recently.[62]

The widths of the exciton absorption and of the band edge luminescence peaks reflect the nanoparticle size polydispersity. In our case, only the defect-state PL was observed. We therefore use the width of the first exciton absorption peak to evaluate the size distribution of the nanoparticles, which is a good indicator for size focusing or defocusing. Due to the difficulty in determining the full width at half-maximum (fwhm), similar to the case of Yu et al.,[63] we measured the half-width at half-maximum (hwhm) on the low-energy side of the first exciton absorption peak for each sample. For all three Cd^{2+}/S^{2-} ratios, we can see a very sharp decrease of hwhms at short aging times, indicating a rapid size focusing, followed by a slow increase of hwhms, indicating a slow size defocusing. For Cd^{2+}/S^{2-} = 1:1, the narrowest hwhm is 14 ± 1 nm, comparable to the 11 ± 1 nm of hwhm for the monodisperse CdS nanocrystals by Yu et al.[63] Note that the largest variation in growth (both the narrowing of the size distribution and the rapid red shift of the band gaps) occurred mainly within 1 day. Therefore the RT growth can be divided into two stages: a fast one within 1 day, due to the focusing growth, and a slow one, due to defocusing growth. Our results agree with recent studies that indicate that the control of the growth behavior can be used to obtain a narrow size distribution.[58,59] In our case, CdS nanoparticles synthesized with stoichiometric ratio had an especially narrow size distribution.

In addition, we also plotted the red shifts and fwhms of the defect-state PL peak energy versus the aging times for a Cd^{2+}/S^{2-} ratio of 3:1. The obvious red shift in the PL peak energy with aging reflects the size sensitivity of this PL band. The narrowest fwhm for the PL is 106 ± 2 nm and much broader than that for the corresponding lowest exciton absorption band (44 ± 2 nm), pointing out its defect-state nature. An interesting feature is that the size-focusing process was additionally observed from the variations in fwhm from the defect-state PL with aging (Figure 6b inset): very small fwhms at short aging times, followed by nearly constant minimum fwhms for longer aging times. The fwhm changes in the PL for shorter time aging agree with the corresponding hwhm changes in the first exciton absorption peaks. This is not true for longer aging times, which we assign to the difference in light absorption and emission processes: Absorption spectra reflect all particles in solution, while PL spectra only represent those that emit radiatively. This might indicate that a narrower size distribution reflects a better surface ordering, therefore decreasing nonradiative processes.

CdS/Dendrimer Nanocomposites

J. Phys. Chem. B, Vol. 109, No. 1, 2005 **235**

Note that the PL yield continuously increases with aging. The increase in PL intensity can be described by two stages. The first stage coincides with the size-focusing stage of particle growth, and the second stage falls in the size-defocusing stage. Recently, several groups have studied the relation between band edge exciton emission and growth conditions of nanocrystals.[64−66] The increasing PL yield during the size-focusing stage has been observed for band edge exciton emission.[64,66] This is ascribed to an optimal surface structure/surface reconstruction of the nanocrystal (less surface defect states) during the focusing growth. We believe that this mechanism is also responsible for the defect-state PL that increases in the first stage in our case. Most probably, mainly nonradiative defect states are eliminated in comparison with the case of band edge exciton emission (where both nonradiative and radiative defect-state emissions are eliminated). Talapin et al. found that during the Ostwald ripening stage, the particles with nearly zero growth rate show the most efficient band edge exciton emission.[65] They claim that this is due to a better surface passivation, obtained by a slower growth rate. For our case, the growth rate is very slow in the second stage, although size defocusing starts due to Ostwald ripening. This translates into a further optimization of the surface and therefore further increase of the PL. Constant minimum fwhms of the PL during the second stage support the results by Talapin et al. For CdS nanoparticles with an initial Cd^{2+}/S^{2-} ratio of 3:1, the PL yield increased (by up to 700%, see Figure 6b). The final quantum yield was 11% at room temperature, compared with coumarin 47. The PL yields for the other samples also increased, by max. 200%.

Influence of Aging on the Blue Photoluminescence. Sooklal et al. first reported strong blue PL from CdS nanoparticles with G4 dendrimers as stabilizers.[23] They found very high room-temperature PL yields. The mechanism of this blue PL has, however, not been elucidated. Three mechanisms can operate for CdS nanoparticles: Recombination of free carriers (A), of trapped holes with free electrons or shallow-trapped electrons (B), and of trapped electrons with free or shallow-trapped holes (C). When free carriers are responsible for the PL, the emission energy $h\nu$ should be close to the band gap E_g. For bulk CdS, the difference between the effective mass of an electron ($m_e = 0.22\, m_0$, where m_0 is the mass of a free electron) and that of a hole ($m_h = 0.7\, m_0$) is relatively large. The fraction of extra energy (due to confinement) carried by electrons is rather high (75%) compared to that carried by holes (25%). This indicates that the recombination of a free electron with a trapped hole (mechanism B) is more sensitive to size effects than that of a trapped electron with a free hole (mechanism C). Therefore, we can use the dependence of the PL peak energy ($h\nu$) on the particle size to distinguish between mechanisms B and C.

As shown above, CdS nanoparticles with nonstoichiometric ratios show an obvious growth behavior. We can use this to study the relation between the PL and the particle size. Figure 7 presents absorption, PL excitation, and emission spectra of CdS/G8NH$_2$ nanocomposites aged for 1 and 22 days in methanol (initial Cd^{2+}/S^{2-} ratio of 3:1). Red shifts of the band gaps and of the PL peaks (see Figure 6) indicate an increase in particle size upon aging. Recently, CdS nanoparticles of similar size (2 nm), obtained from a high-temperature synthesis, have been reported to show only band edge PL.[62] The strong band edge emission of such small CdS nanoparticles (2.6 nm) was further verified by Yu et al., although the defect-state PL still has 12% room-temperature quantum yield, indicating the difficulty in getting rid of the defect-state emission from very small nanoparticles.[51]
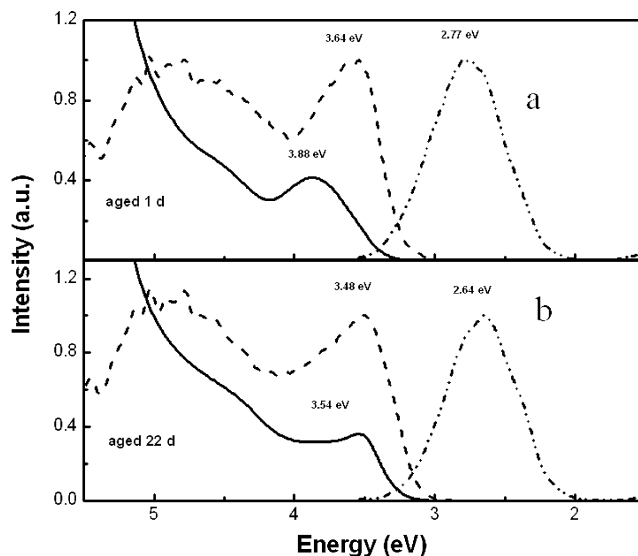

Figure 7. Absorption (solid lines), excitation ($\lambda_{em} = 450$ nm, dashed lines), and PL ($\lambda_{ex} = 320$ nm, dashed dotted lines) spectra of CdS nanoparticles aged 1 day (top) and 22 days (bottom).

We did not obtain band edge emission, probably because our CdS has more defects due to imperfect surface passivation, and due to the low synthesis temperature. Our excitation band gaps were narrower than the absorption band gaps, indicating less effective emission from smaller particles. We therefore used the excitation band gap E_g in the following calculations. We found $E_g - h\nu = 0.87 \pm 0.005$ eV for 1 day and 0.84 ± 0.005 eV for 22 days aging ($h\nu$ is the PL peak energy). Since $E_g - h\nu$ is quite large, we can exclude mechanism A. Therefore, the PL process should involve deep-trapped electrons or holes. For a transition arising from a trapped electron and a free hole, the variation of $h\nu$ with particle size ($\Delta h\nu$) would be close to 0.25 ΔE_g (ΔE_g is the variation of E_g with the particle size) since the hole carries 25% extra energy, as discussed above. $\Delta h\nu$ between Figure 7a and Figure 7b (0.13 eV) was, however, rather close to $0.75\Delta E_g = 0.12$ eV, indicating its high sensitivity to the particle size. From this, we can exclude trapped electrons (mechanism C) as deep-trapped carriers here.

Therefore, mechanism B is the most probable pathway for the PL process. For mechanism B, the energy level difference between the trapped hole and the valence band caused by size variations should be close to $0.25\Delta E_g$. The difference between the 0.87 eV determined from Figure 7a and the 0.84 eV from Figure 7b is 0.03 eV, in good agreement with the value of $0.25\Delta E_g$ (0.04 eV). For bulk CdS, a deep-trapped hole state $\sim$0.84 eV above the valence band[67] fits to the PL energy value we observed here. Mechanism B is also reported to be responsible for the trapped-state PL in CdS nanoparticles synthesized with other stabilizers.[41,68,69] For example, Haesselbarth et al. used two different electron acceptors to quench the PLs from CdS nanoparticles stabilized by Na$_4$P$_2$O$_7$ in aqueous solution. By the comparison between the electron trap potential and the acceptor potentials, they verified that the electron traps are shallow and that defect-state PL involves shallow electron traps and deep hole traps, located on the surface of the nanocrystalline particles.[68] Lifshitz et al. performed photoluminescence and optically detected magnetic resonance studies; they verified that trapped-state PL results from recombination between shallow-trapped electrons and deep-trapped holes, associated with the surface of the particles.[69]
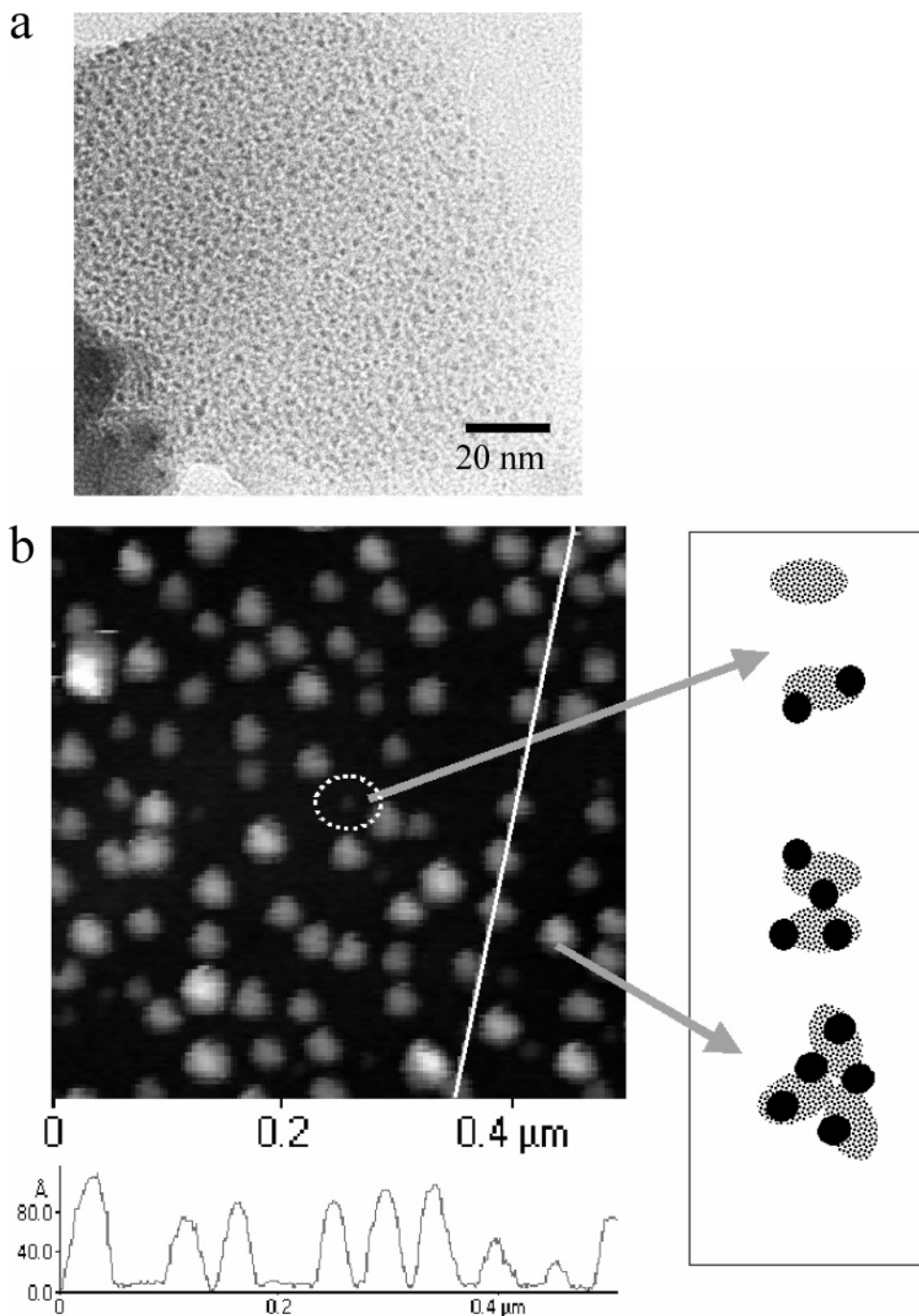
Figure 8. (a) Transmission electron micrograph of CdS/G8NH$_2$ nanocomposites. (b) Topographic IC-AFM images (intermittent contact mode) of CdS/G8NH$_2$ nanocomposites (initial Cd^{2+}/S^{2-} ratio of 3:1) on a silicon wafer after adsorption from solution. The white line is the topographic profile shown below. Right: Illustration of possible nanocomposites. (See text.)

5. Morphology and Adsorption

Since we used a Cd^{2+}/G8NH$_2$ ratio of 360 for the synthesis, Cd^{2+} should bind only to the terminal NH$_2$ groups (1024 per molecule), and the nucleation sites of the CdS nanoparticles should be the NH$_2$ groups. Therefore, the location of the CdS nanoparticles is most probably at the surface region of the dendrimers; i.e., the CdS nanoparticles are bound to the NH$_2$ groups. The diameter of the particles calculated from the absorption band gap is ≤ 2 nm,[63] which is smaller than the 3.4 nm calculated by assuming one particle (Cd$_{360}$S$_{360}$) per G8NH$_2$. The transmission electron micrograph shown in Figure 8a also verifies the size of the CdS nanoparticles (around 1.5 nm). The synthesized CdS nanocomposites are therefore of the external type, with roughly two CdS nanoparticles per dendrimer

(estimated). Figure 8b presents a topographic intermittent contact (IC) AFM image of nanocomposites on an oxidized silicon wafer. The average height of the nanocomposites is ∼9 nm; they have a relatively narrow size distribution and a regular shape. There are some 3−4 nm high small dots (see circle). This height corresponds to that of single G8NH$_2$ molecules on hydrophilic substrates.[68−70] Such a dot can be either a single pure G8NH$_2$ or a single G8NH$_2$ with CdS nanoparticles. Thus, our 9 nm average height indicates that most isolated dots in the AFM image contain two or three G8NH$_2$ molecules together with several CdS nanoparticles.

Adsorption of Cd*S*/Dendrimer Nanocomposites on Flat Substrates. The adsorption of pure dendrimers on substrates can be classified into two types. On hydrophilic substrates, single
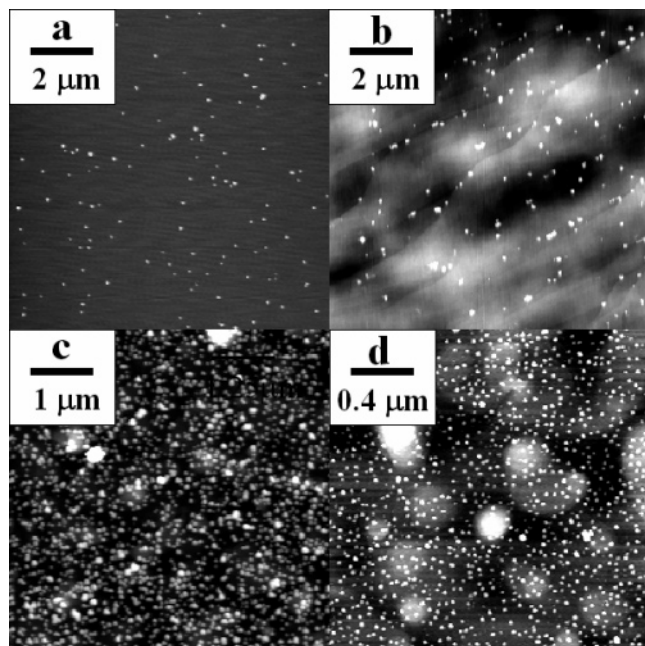
Figure 9. Topographic IC-AFM images of CdS/G8NH$_2$ nanocomposites adsorbed on (a) mica, (b) graphite, (c) gold, and (d) HOOC(CH$_2$)$_{15}$S/gold.

Figure 10. Topographic IC-AFM images of CdS/G8NH$_2$ nanocomposites printed on gold/chromium/glass substrates (3 μm pattern size).

dendrimers dominate; their AFM-determined height is smaller than their diameters in solution, indicating a deformation due to strong interactions between dendrimers and substrate.[70−72] On hydrophobic substrates, aggregates of several or even tens of dendrimers dominate, but the height of a single dendrimer is similar to its diameter in solution, indicating weak dendrimer−substrate interactions.[70]

We imaged fresh CdS/G8NH$_2$ nanocomposites on mica with AFM (see Figure 9). Compared to the silicon wafer (Figure 8b), the coverage of CdS/G8NH$_2$ on mica was much lower, despite the high hydrophilicity of the mica substrate. The particle sizes on mica were larger than on silicon, indicating the formation of aggregates. This is different from the adsorption of pure NH$_2$-terminated (or NH$_3^+$-terminated) dendrimers on mica, where single dendrimers dominate.[70,73] The difference between a silicon wafer and mica may be due to the higher density of OH groups on the wafer.

Pure graphite showed some (multilayer) steps. After adsorption of CdS/G8NH$_2$ nanocomposites, the substrate was covered with spots (see white dots in Figure 9b; some graphite steps extend from the lower left to the upper right). Compared with CdS/G8NH$_2$ on a silicon wafer, the spots were larger in size and less regular in shape, indicating further agglomeration of nanocomposites upon adsorption. CdS nanoparticles should not play a role in this agglomeration process since pure dendrimers, too, exist mainly in the form of aggregates on a hydrophobic substrate.[73]

Nanocomposites can also adsorb on pure gold and on a self-assembled monolayer, HOOC(CH$_2$)$_{15}$S/gold (Figure 9c,d; the gray or white islands with >200 nm diameter result from the gold morphology). Since pure G8NH$_2$ adsorbs on gold with multidentate Au−NH$_2$ interactions,[72,74] we assume a similar mechanism for the adsorption of CdS/G8NH$_2$ nanocomposites on gold. For the carboxylate-terminated molecular layer, electrostatic forces—in addition to hydrogen bonds—can also be important: Partial deprotonation of COOH groups produces a negatively charged surface, while partial protonation of NH$_2$ groups results in positively charged nanocomposites.[32]
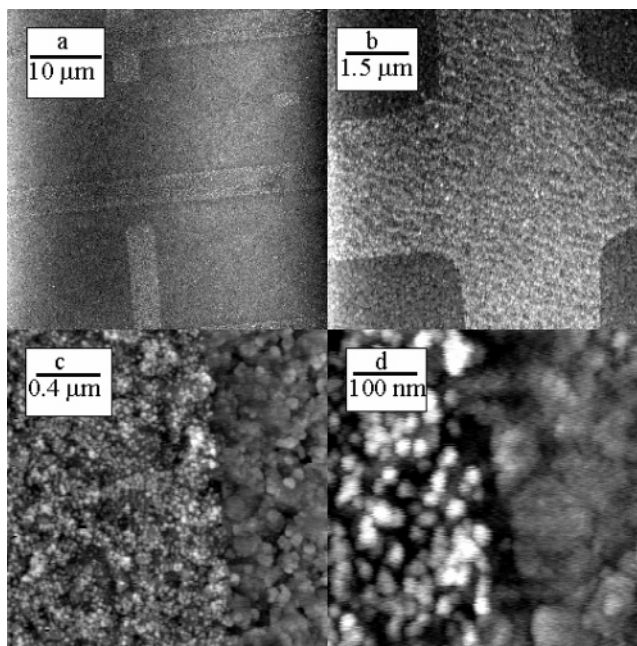
From these observations, we can roughly classify the adsorption of fresh CdS/G8NH$_2$ nanocomposites into two types, according to their interaction with the substrate: When hydrogen bonds, multidentate metal−ligand interactions, or electrostatic forces prevail, the composites will adsorb strongly and will not form large aggregates. Substrates that belong to this type are silicon, gold, and carboxylate-terminated substrates (mica, although hydrophilic, does not fit very well into this category). In contrast, when nanocomposites interact weakly (by van der Waals forces) with hydrophobic substrates such as graphite, the particles can diffuse on the substrate and form larger aggregates.[73]

On the basis of these findings, our CdS/G8NH$_2$ nanocomposites should be patterned on substrates in the same way as pure dendrimers. Indeed we have successfully patterned CdS/G8NH$_2$ nanocomposites on silicon wafers, on the basis of interactions between NH$_2$ groups (of G8NH$_2$) and OH groups on the silicon surface.[75] Similarly, dendrimers form a monolayer on gold (due to multidentate Au−NH$_2$ interactions) when adsorbed from solution.[71,73] The nanocomposites, too, show a high coverage after adsorption on gold (Figure 9c). Hence, they should be printable on gold, which we demonstrate in Figure 10. The large scan (Figure 10a) indicates a successful transfer of the nanocomposites to the gold surface. Zoom-in scans (Figure 10b,c,d) suggest a high coverage in the printed (contact) region and a sharp edge between the printed and the unprinted regions.

6. Conclusions

Amine-terminated polyamidoamine dendrimers of generation 8 (G8NH$_2$) can be used as stabilizers for the synthesis of very small CdS nanoparticles from Cd^{2+} and S^{2-} in methanol at 25 °C. The particles are located at the surface regions of the dendrimers and can be further modified by amines, thiols, and metal ions. Sequential addition of S^{2-} and Zn^{2+} yields CdS−ZnS core−shell nanocomposites. Blue photoluminescence (PL) is the dominant PL in this system and is most efficient when the ratio Cd^{2+}/S^{2-} is at least 1.5 in the synthesis. Energy level structure analysis and picosecond time-resolved PL decay

measurements indicate that deep-trapped holes (Cd^{2+} vacancies) recombine with shallow-trapped or free electrons to yield the blue PL. Shallow hole traps dominate the nonradiative processes. By controlling the nonradiative pathways, e.g., with added Cd^{2+}, the blue PL can be improved.

Through the control of the preparation conditions, very small CdS nanoparticles (2 nm in diameter) with a narrow size distribution can be obtained. Their structure is presumably imperfect; consequently the PL is dominated by a defect-state emission. We show that additives can passivate various possible defect states at the surface of the CdS nanoparticles.

The interaction between our CdS/G8NH$_2$ nanocomposites and various flat substrates allows for dendrimer-induced facile adsorption via hydrogen bridges or multidentate metal−ligand or electrostatic interactions. This constitutes the basis for the printing of nanocomposites on hydrophilic substrates.[75] Hence, one material (the dendrimers) can fulfill two functions, acting as nanoparticle stabilizer in their synthesis and allowing nanoparticle binding to flat substrates. The method that we present could be widely applied; for example, one could replace the stabilizers of other nanoparticles by carboxylate- and amine-terminated dendrimers in a simple reaction.[4,66,76] The resulting particles can thereafter be immobilized by adsorption or by printing on a range of substrates.

Appendix: Calculation of the Thickness of ZnS and PbS Shells

M_{CdS}, d_{CdS}, and n_{CdS} are molecular weight, density, and the number of MS (metal particles sulfide) per nm^3, respectively.
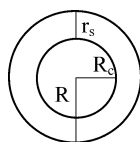
$$n_{CdS} = (6.02 \times 10^{23}/mol)(1/M_{CdS})d_{CdS}$$

$$= (6.02 \times 10^{23}/mol)[1/(144.48 \text{ g/mol})](4.83 \text{ g/cm}^3)$$

$$= 20/nm^3$$

Similarly,

$$n_{ZnS} = (6.02 \times 10^{23}/mol)(1/M_{ZnS})d_{ZnS}$$

$$= (6.02 \times 10^{23}/mol)[1/(97.456 \text{ g/mol})](4.09 \text{ g/cm}^3)$$

$$= 25/nm^3$$

Similarly,

$$n_{PbS} = (6.02 \times 10^{23}/mol)(1/M_{PbS})d_{PbS}$$

$$= (6.02 \times 10^{23}/mol)[(1/(239.27 \text{ g/mol})](7.6 \text{ g/cm}^3)]$$

$$= 19/nm^3$$

Supposing that the concentration of M^{2+} ions in solution, the number of nanoparticles in solution, the volume of the nanoparticle, and the number of MS per nanoparticle are $C_{M^{2+}}$, X_{MS}, V ($V = (4/3)\pi R_C^3$), and N_{MS} ($=Vn_{MS}$), respectively, then

$$X_{CdS} = (6.02 \times 10^{23}/mol)(C_{Cd^{2+}}/N_{CdS})$$

$$X_{ZnS} = (6.02 \times 10^{23}/mol)(C_{Zn^{2+}}/N_{ZnS})$$

If we assume that the entire amount of ZnS grows exclusively on the CdS cores, then $X_{CdS} = X_{ZnS}$. The result is as follows:

$$C_{Zn^{2+}}/C_{Cd^{2+}} = N_{ZnS}/N_{CdS} = (R^3 - R_C^3)n_{ZnS}/R_C^3 n_{CdS}$$

$$R = [1 + 0.8(C_{Zn^{2+}}/C_{Cd^{2+}})]^{1/3}R_C$$

For the PbS shell:

$$R = [1 + 0.8(C_{Pb^{2+}}/C_{Cd^{2+}})]^{1/3}R_C$$

References and Notes

(1) Henglein, A. *Top. Curr. Chem.* **1988**, *143*, 113. Alivisatos, A. P. *Science* **1996**, *271*, 933. Steigerwald, M. L.; Brus, L. E. *Acc. Chem. Res.* **1990**, *23*, 183; Chestnoy, N.; Harris, T. D.; Brus, L. E. *J. Phys. Chem.* **1986**, *90*, 3393.
(2) Bawendi, M. G.; Steigerwald, M. L.; Brus, L. E. *Annu. Rev. Phys. Chem.* **1990**, *41*, 477.
(3) Murray, C. B.; Norris, D. J.; Bawendi, M. G. *J. Am. Chem. Soc.* **1993**, *115*, 8706.
(4) Peng, X. G.; Schlamp, M. C.; Kadavanich, A. V.; Alivisatos, A. P. *J. Am. Chem. Soc.* **1997**, *119*, 7019.
(5) Peng, Z. A.; Peng, X. G. *J. Am. Chem. Soc.* **2001**, *123*, 183.
(6) Peng, Z. A.; Peng, X. G. *J. Am. Chem. Soc.* **2002**, *124*, 3343.
(7) Spanhel, L.; Hasse, M.; Weller, H.; Henglein, A. *J. Am. Chem. Soc.* **1987**, *109*, 5649.
(8) Gaponik, N.; Talapin, D. V.; Rogach, A. L.; Hoppe, K.; Shevchenko, E. V.; Kornowski, A.; Eychmüller, A.; Weller, H. *J. Phys. Chem. B* **2002**, *106*, 7177.
(9) Pileni, M. P. *Catal. Today* **2000**, *58*, 151.
(10) Zhao, H.; Douglas, E. P.; Harrison, B. S.; Schanze, K. S. *Langmuir* **2001**, *17*, 8428.
(11) Zhou, H. S.; Honma, I.; Komiyama, H.; Haus, J. W. *J. Phys. Chem.* **1993**, *97*, 895.
(12) Vossmeyer, T.; Jia, S.; Delono, E.; Diehl, M. R.; Kim, S. H.; Peng, X.; Alivisatos, A. P.; Heath, J. R. *J. Appl. Phys.* **1998**, *84*, 3664.
(13) Rogach, A. L.; Susha, A. S.; Caruso, F.; Sukhorukov, G. B.; Kornowski, A.; Kershaw, S.; Möhwald, H.; Eychmüller, A.; Weller, H. *Adv. Mater.* **2000**, *12*, 333.
(14) Lu, C.; Wu, N.; Wei, F.; Zhao, X.; Jiao, X.; Xu, J.; Luo, C.; Cao, W. *Adv. Funct. Mater.* **2003**, *13*, 548.
(15) Tomalia, D. A.; Baker, H.; Dewald, J.; Hall, M.; Kallos, G.; Martin, S.; Roeck, J.; Ryder, J.; Smith, P. *Polym. J.* **1985**, *17*, 117.
(16) Balogh, L.; Tomalia, D. A. *J. Am. Chem. Soc.* **1998**, *120*, 7355.
(17) Zhao, M. Q.; Crooks, R. M. *J. Am. Chem. Soc.* **1998**, *120*, 4877.
(18) Zhao, M. Q.; Crooks, R. M. *Angew. Chem., Int. Ed.* **1999**, *38*, 364.
(19) Lemon, B. I.; Crooks, R. M. *J. Am. Chem. Soc.* **2000**, *122*, 12886.
(20) Zhao, M. Q.; Crooks, R. M. *Chem. Mater.* **1999**, *11*, 3379.
(21) Zheng, J.; Stevenson, M. S.; Hikida, R. S.; Van Patten, P. V. *J. Phys. Chem. B* **2002**, *106*, 1252.
(22) Strable, E.; Bulte, J. M.; Moskowitz, B.; Vivekanandan, K.; Allen, M.; Douglas, T. *Chem. Mater.* **2001**, *13*, 2201.
(23) Sooklal, K.; Hanus, L. H.; Ploehn, H. J.; Murphy, C. J. *Adv. Mater.* **1998**, *10*, 1083.
(24) Huang, J. M.; Sooklal, K.; Murphy, C. J. *Chem. Mater.* **1999**, *11*, 3595.
(25) Hanus, L. H.; Sooklal, K.; Murphy, C. J.; Ploehn, H. J. *Langmuir* **2000**, *16*, 2621.
(26) Tan, N. C. B.; Balogh, L.; Trevino, S. F.; Tomalia, D. A.; Lin, J. S. *Polymer* **1999**, *40*, 2537.
(27) Donners, J. J. J. M.; Hoogenboom, R.; Schenning, A. P. H. J.; Hal, P. A. van.; Nolte, R. J. M.; Meijer, E. W.; Sommerdijk, N. A. J. *Langmuir* **2002**, *18*, 2571.
(28) Balogh, L.; Valluzzi, R.; Laverdure, K. S.; Gido, S. P.; Hagnauer, G. L.; Tomalia, D. A. *J. Nanopart. Res.* **1999**, *1*, 353.
(29) Tsukruk, V. V.; Rinderspacher, F.; Bliznyuk, V. N. *Langmuir* **1997**, *13*, 2171.
(30) Zhang, H.; Grim, P. C. M.; Liu, D.; Vosch, T.; De Feyter, S.; Wiesler, U. M.; Berresheim, A. J.; Müllen, K.; Haesendock, C. V.; Vandamme, N.; De Schryver, F. C. *Langmuir* **2002**, *18*, 1801.
(31) Lackowski, W. M.; Campbell, J. K.; Edwards, G.; Checkik, V.; Crooks, R. M. *Langmuir* **1999**, *15*, 7632.
(32) Manríquez, J.; Juaristi, E.; Muñoz-Muñiz, O.; Godínez, L. A. *Langmuir* **2003**, *19*, 7315.
(33) Watanabe, S.; Regen, S. *J. Am. Chem. Soc.* **1994**, *116*, 4877.
(34) Wu, X. C.; Bittner, A. M.; Kern, K. *Langmuir* **2002**, *18*, 4984.

(35) Arrington, D.; Curry, M.; Street, S. C. *Langmuir* **2002**, *18*, 7788.

(36) Li, H. W.; Kang, D. J.; Blamire, M. G.; Huck, W. T. S. *Nano Lett.* **2002**, *2*, 347.

(37) Youn, H. C.; Baral, S.; Fendler, J. H. *J. Phys. Chem.* **1988**, *92*, 6320.

(38) Haesselbarth, A.; Eychmüller, A.; Eichberger, R.; Giersig, M.; Mews, A.; Weller, H. *J. Phys. Chem.* **1993**, *97*, 5333.

(39) Mews, A.; Eychmüller, A.; Giersig, M.; Schooss, D.; Weller, H. *J. Phys. Chem.* **1994**, *98*, 934.

(40) Mews, A.; Kadavanich, A. V.; Banin, U.; Alivisatos, A. P. *Phys. Rev. B* **1996**, *53*, R13242.

(41) Cizeron, J.; Pileni, M. P. *J. Phys. Chem. B* **1997**, *101*, 8887.

(42) Carrot, G.; Scholz, S. M.; Lummer, C. J. G.; Hilborn, J. G.; Hedrick, J. L *Chem. Mater.* **1999**, *11*, 3571.

(43) Ottaviani, M. F.; Montalti, F.; Turro, N. J.; Tomalia, D. A. *J. Phys. Chem. B* **1997**, *101*, 158.

(44) Guilbault, G. G.; Billedeau, S. M. *J. Inorg. Nucl. Chem.* **1972**, *34*, 1167.

(45) Hines. M. A.; Guyot-Sionnest, P. *J. Phys. Chem.* **1996**, *100*, 468.

(46) Dabbousi, B. O.; Rodriguez-Viejo, J.; Mikulec, F. V.; Heine, J. R.; Mattoussi, H.; Ober, R.; Jensen, K. F.; Bawendi, M. G. *J. Phys. Chem. B* **1997**, *101*, 9463.

(47) Peng, X. G.; Schlamp, M. C.; Kadavanich, A. V.; Alivisatos, A. P. *J. Am. Chem. Soc.* **1997**, *119*, 7019.

(48) Dag, I.; Lifshitz, E. *J. Phys. Chem.* **1996**, *100*, 8962.

(49) Burda, C.; Link, S.; Mohamed, M.; El-Sayed, M. *J. Phys. Chem. B* **2001**, *105*, 12286.

(50) Underwood, D. F. Kippeny, T. Rosenthal, S. *J. Phys. Chem. B* **2001**, *105*, 436.

(51) Yu, Z. H.; Li, J. B.; O'Connor, D. B.; Wang, L. W.; Barbara, P. F. *J. Phys. Chem. B* **2003**, *107*, 5670.

(52) Chestnoy, N.; Harris, T. D.; Brus, L. E. *J. Phys. Chem.* **1986**, *90*, 3393.

(53) Lakowicz, J. R.; Gryczynski, I.; Gryczynski, Z.; Murphy, C. J. *J. Phys. Chem. B* **1999**, *103*, 7613.

(54) Haus, J. W.; Zhou, H. S.; Honma, I.; Komiyama, H. *Phys. Rev. B* **1993**, *47*, 1358.

(55) LaMer, V. K.; Dinegar, R. H. *J. Am. Chem. Soc.* **1950**, *72*, 4847.

(56) Sugimoto, T. *Adv. Colloid Interface Sci.* **1987**, *28*, 65.

(57) Peng, X. G.; Wickham, J.; Alivisatos, A. P. *J. Am. Chem. Soc.* **1998**, *120*, 5343.

(58) Talapin, D. V.; Rogach, A. L.; Haase, M.; Weller, H. *J. Phys. Chem. B* **2001**, *105*, 12278.

(59) Ingert, D.; Feltin, N.; Levy, L.; Gouzerh, P.; Pileni, M. P. *Adv. Mater.* **1999**, *11*, 220.

(60) Vossmeyer, T.; Katsikas, L.; Giersig, M.; Popovic, I. G.; Diesner, K.; Chemseddine, A.; Eychmüller, A.; Weller, H. *J. Phys. Chem.* **1994**, *98*, 7665.

(61) Herron, N.; Calabrese, J. C.; Farneth, W. E.; Wang, Y. *Science* **1993**, *259*, 1426.

(62) Yu, W. W.; Peng, X. G. *Angew. Chem., Int. Ed.* **2002**, *41*, 2368.

(63) Yu, W. W.; Qu, L. H.; Guo, W. Z.; Peng, X. G. *Chem. Mater.* **2003**, *15*, 2854.

(64) Qu, L. H.; Peng, X. G. *J. Am. Chem. Soc.* **2002**, *124*, 2049.

(65) Talapin, D. V.; Rogach, A. L.; Shevchenko, E. V.; Kornowski, A.; Hasse, M.; Weller, H. *J. Am. Chem. Soc.* **2002**, *124*, 5782.

(66) Donega, C. M.; Hickey, S. G.; Wuister, S. F.; Vanmaekelbergh, D.; Meijerink, A. *J. Phys. Chem. B* **2003**, *107*, 489.

(67) Ralph, J. E. *Solid State Commun.* **1978**, *28*, 377.

(68) Haesselbarth, A.; Eychmueller, A.; Weller, H. *Chem. Phys. Lett.* **1993**, *203*, 271.

(69) Lifshitz, E.; Glozman, A.; Litvin, I. D.; Porteanu, H. *J. Phys. Chem. B* **2000**, *104*, 10449.

(70) Li, J.; Piehler, L. T.; Baker, J. R.; Tomalia, D. A. *Langmuir* **2000**, *16*, 5613.

(71) Hielerman, A.; Campbell, J. K.; Baker, L. A.; Crooks, R. M.; Ricco, A. J. *J. Am. Chem. Soc.* **1998**, *120*, 5323.

(72) Betley, T. A.; Holl, M. M. B.; Orr, B. G.; Swanson, D. R.; Tomalia, D. A.; Baker, J. R. *Langmuir* **2001**, *17*, 2768.

(73) Müller, T.; Yablon, D. G.; Karchner, R.; Knapp, D.; Kleinman, M. H.; Fang, H.; Durning, C. J.; Tomalia, D. A.; Turro, N. J.; Flynn, G. W. *Langmuir* **2002**, *18*, 7452.

(74) Chechik. V.; Zhao, M. Q.; Crooks, R. M *J. Am. Chem. Soc.* **1999**, *121*, 4910.

(75) Wu, X. C.; Bittner, A. M.; Kern, K. *Adv. Mater.* **2004**, *16*, 413.

(76) Schmelz, O.; Mews, A.; Basche, T.; Herrmann, A.; Müllen, K. *Langmuir* **2001**, *17*, 2861.